Robot and overhead crane collaboration scheme to enhance payload manipulation

Antonio Rosales, Alaa Abderrahim and Markku Suomalainen
VTT Technical Research Centre of Finland Ltd., Oulu, Finland

Mikael Haag
Konecranes Oyj, Hyvinkää, Finland, and

Tapio Heikkila
VTT Technical Research Centre of Finland Ltd., Oulu, Finland

Abstract

Purpose – This paper aims to present a scheme to enhance payload manipulation using a robot collaborating with an overhead crane. In the current industrial practice, when the crane's payload has to be accurately manipulated and located in a desired position, the task becomes laborious and risky as the operators have to guide the fine motions of the payload by hand. In the proposed collaborative scheme, the crane lifts the payload while the robot's end-effector guides it toward the desired position.

Design/methodology/approach – Two admittance transfer functions are considered to accomplish harmless and smooth contact with the payload. The first admittance is used in a velocity-based admittance control integrated with the robot. The second one adds compliance to the crane by processing the interaction force through the admittance transfer function to generate a crane's velocity command that makes the crane follow the payload.

Findings – The robot's end-effector and the crane move collaboratively to guide the payload to the desired location. A method is presented to design the admittance controllers that accomplish a fluent robot-crane collaboration. Simulations and experiments validating the scheme potential are shown.

Originality/value – This paper presents a new collaborative scheme robot-crane to manipulate heavy loads. The only link between the robot and the crane is the interaction force produced during the guiding of the payload.

Keywords Cooperating robots, Compliance and impedance control, Industrial robots

Paper type Research paper

1. Introduction

Overhead cranes are essential for lifting and moving weighty payloads in heavy manufacturing industries. When the payload needs to be located at a specific place or positioned at a desired pose, the crane's operator manually guides the payload either pushing or pulling to get the desired position. This manual guiding is mainly made with one hand while the other is used to operate the crane's control. Manual assistance requires skilled persons to be found and/or trained representing a time consumption not always welcome for the tight industrial production schedules Hoffman and Asada (2020). Also, manual guiding might compromise the safety of the operators Bey-Temsamani *et al.* (2022), and if the guiding is not executed precisely, the payload might be damaged Hoffman and Asada (2021).

Increasing the automation levels in overhead cranes is needed to ensure payload manipulation without risking the operator and the payload. Automation of payload manipulation has been carried out by integrating robotic and mechatronic systems with cranes. One approach is cable-driven parallel robotic systems combined with current overhead crane technologies. This approach is presented in Hoffman and Asada (2020, 2021); O'Neill and Asada (2021, 2022) accomplishing fully automated insertion tasks only analyzing the cable tension forces. However, a fully automated solution misses human guidance and supervision capabilities.

Another approach to automate overhead cranes is using Intelligent Assist Devices (IAD) Krüger *et al.* (2009). IAD are widely used in industrial applications to assist the operator in

The current issue and full text archive of this journal is available on Emerald Insight at: **https://www.emerald.com/insight/0143-991X.htm**

Industrial Robot: the international journal of robotics research and application
Emerald Publishing Limited [ISSN 0143-991X]
[DOI 10.1108/IR-07-2025-0229]

Funding: HORIZON EUROPE Digital, Industry and Space, 101007311. This work was supported by the INVERSE Project under Grant 101136067 funded by the European Union.

Received 1 July 2025
Revised 31 October 2025
Accepted 3 November 2025

moving and lifting the payload Bicchi *et al.* (2008), these devices transform the operator's forces and/or changes of payload's positions into crane commands. Considering the type of apparatus used to assist the crane, the IAD can be divided into two groups. One group uses handles or levers that map the force exerted on them to crane motion commands. The second group uses a robot arm to move the payload lifted by the crane.

Most of the IAD presented in the literature use handles/levers. In Campeau-Lecours *et al.* (2017), the pulling and pushing forces at the device's assistance are measured and analyzed but these forces are not used in the robot controller. In Campeau-Lecours *et al.* (2016), the authors integrate admittance force control to the approach in Campeau-Lecours *et al.* (2017), but no details about the design of the admittance controller are provided. The assistance device presented in Welch *et al.* (2022) uses admittance control including stability analysis; however, the accuracy of the payload position is compromised since the operator sets the desired position via his/her visual feedback. Another approach that fits in the IAD using handles/levers is the work in Peng *et al.* (2009). The authors used a tag held by the operator to sense three-dimensional motion and the sensed motion is used to command the crane. However, the method lacks the advantage of guiding the load directly since the operator indirectly guides the payload via the handled tag.

A few works focus on using a robot as an IAD, and most of them are based on constraint motion, i.e. only position/velocity control is used for controlling the interaction between robot and payload, see Ambrosino *et al.* (2022, 2024); Heuer and Brell-Cokcan (2025b); Liu *et al.* (2024). In Schubert *et al.* (2019), a robot operated with a joystick is the assistant device. Force feedback between the assistance device (robot) and the joystick is considered, but the robot's and the crane's interaction is based on constraint motion. Using constraint motion to execute interaction tasks is not recommended, as contact forces can increase and saturate the robot's actuators or the object in contact can be damaged Siciliano *et al.* (2009). In Arai *et al.* (1988), the IAD is a robot with a flexible link to add compliance and move the crane's payload smoothly. The signal of a strain gauge mounted at the flexible link is used to sense the interaction between the robot and the payload. The main drawback of the approach is the flexible link as oscillations may occur and changing the stiffness requires a physical modification of the robot. Also, patents are addressing the manipulation of heavy loads considering a crane collaborating with a robot, and using force measurements (Kazuo *et al.*, 1994; Kazuo and Shinsaku, 1995; Yutaka and Motohisa, 1994); however, the patents omit details of the controller used for mapping force to velocity. In construction applications (Heuer and Brell-Cokcan, 2025a), robots with passive compliance mechanisms are used as IAD, but the interaction forces are not used to control the crane.

This paper presents a novel robot and crane collaborative scheme to manipulate payloads integrating for first-time compliance into the crane via admittance control. The scheme considers a robot guiding a payload lifted by the crane. The crane and robot's end-effector move collaboratively to drive the payload at a desired velocity. The collaboration is based on the interaction force between the robot's end-effector and the payload. The robot and the crane are integrated with admittance controllers to accomplish a soft and safe interaction. The interaction force is measured and used to implement a velocity-based admittance controller in the robot. On the crane side, the measured force is converted into the crane's velocity commands through an admittance transfer function. The design and stability analysis of the admittance controllers are presented. The functionality of the scheme is validated via simulations and experiments.

Compared with the IAD approaches using handlers/levers presented in Campeau-Lecours *et al.* (2017, 2016), Welch *et al.* (2022) and Peng *et al.* (2009). The proposed scheme is harmless for the operator as the robot interacts directly with the payload, and the operator can supervise the manipulation or command the robot using a joystick from a risk-free place. Also, in comparison with the fully automated methods presented in Hoffman and Asada (2020, 2021) and O'Neill and Asada (2021, 2022), the proposed scheme does not remove the valuable skills and experience of the operator as he/she can still supervise or manipulate the robot. Considering the IAD using a robot presented in Schubert *et al.* (2019) and Arai *et al.* (1988), this approach includes compliance in the robot and crane via admittance control offering an accessible way to modify stiffness and damping. Furthermore, the paper presents the design and stability analysis of the admittance controls implemented on the robot and the crane.

The structure of the paper is the following. Section 2 contains the description of the proposed robot crane collaboration scheme. The design and analysis of the scheme are presented in Section 3. Section 4 includes the simulation and experiments, and the discussion and conclusions are in Sections 5 and 6, respectively.

2. Problem statement

Consider a robot in contact with a payload lifted by a crane, see Figure 1(a). The goal is to use the robot to guide the payload from a starting point S to a final point G, while the crane lifts the payload, i.e. the robot collaborates with the crane to accurately locate the payload in a target position. The robot and crane collaboration is based on the contact force exerted on the payload by the robot's end-effector. The payload can be guided in three directions (x, y, z), and the motion control in each direction is decentralized, e.g. no direct communication between each controller. The decentralized guiding is easy to accomplish by controlling the robot and crane in Cartesian space. In the paper,

Figure 1 (a) Sketch of robot-crane collaborative task; (b) pendulum model and contact forces

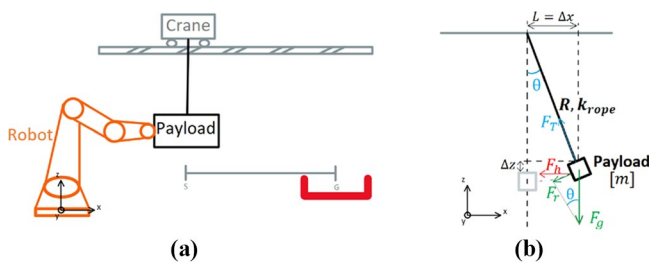

we use the horizontal direction x to describe the proposed approach; however, the collaborative scheme is implemented and tested on the plane xz (see Section 4), and the 3D space xyz extension is discussed in Section 5.

Consider the robot's end-effector exerts a force on the payload along horizontal direction x producing an angle θ measured from the vertical position, see Figure 1(b). The displacement on x direction can be analyzed using a pendulum model. The payload's mass m is the pendulum's mass, R is the length of a mass-less rope and k_{rope} is the rope constant. θ represents the sway angle, L is the horizontal displacement, F_g is the gravity force, F_T is tension along the rope, F_r is the pendulum's restoring force and F_h is the horizontal force applied at the end-effector. Considering $F_g = mg$, with g the earth's gravity, $F_R = -F_g \sin\theta$, $F_T = k_{rope}\Delta z$, and $\theta = \arcsin\left(\frac{L}{R}\right)$, the horizontal force F_h is computed as follows:

$$F_h = F_R\cos\theta + F_T\sin\theta = \sin\theta(-F_g\cos\theta + F_T) \tag{1}$$

The force F_h can be studied as an elastic interaction force F between the robot and the crane. Replacing $\sin\theta$ with $\frac{L}{R}$, one gets $F_h = \frac{L}{R}(-F_g\cos\theta + F_T)$, and the model of the interaction force is as follows:

$$F = K_e\Delta x \tag{2}$$

where $\Delta x = L$ is the difference between the positions of the end-effector/payload and the crane along the x-axis [see Figure 1(b)], and $K_e = (F_T - mg\cos\theta)/R$ is the environment's stiffness. Note that the displacement Δx is directly related to the angle θ. When $\theta = 0$, $\Delta x = 0$ as the crane and end-effector are in the same position. The angle $\theta \neq 0$, when there is a difference in the position of the end-effector/payload compared with the crane, caused by the robot pushing the payload along the x axis. Also, one can see that the environment's stiffness K_e depends on the payload mass m and the rope length R, the heavier the mass and the shorter the rope, the stiffer the environment.

A collaborative scheme with two admittance controllers is proposed to achieve a smooth robot-crane collaboration when the payload is manipulated. The block diagram of the scheme is presented in Figure 2. On the robot side, a velocity-based admittance control (Vukobratovic *et al.*, 2009), ensures harmless contact with the payload while a desired position x_d or velocity v_{x_d} is reached. The admittance transfer function integrated into the robot's control loop makes the robot behave like a mass-spring-damper system with parameters M_r, B_r and K_r to be selected. On the crane side, the admittance transfer function with parameters M_c, B_c and K_c transforms the interaction force F into velocity commands v_{ac} needed to track the velocity set by the robot. The transformed velocity v_{ac} is characterized by the mass-spring-damping response defined by M_c, B_c and K_c. The interaction force F is the only signal connecting the robot with the crane.

Figure 2 Block diagram of the collaborative scheme

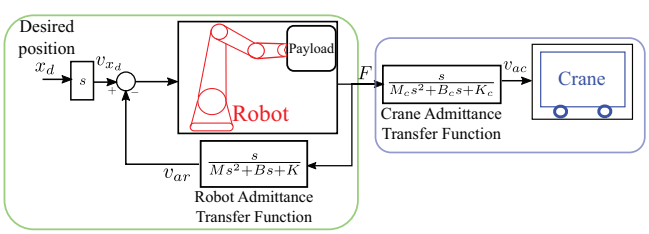

The next section presents how the admittance parameters M_r, B_r, K_r, M_c, B_c and K_c should be selected to accomplish payload manipulation via robot-crane collaboration.

3. Robot-crane collaboration scheme

This section describes the details of the proposed robot-crane collaboration scheme. First, the admittance controllers implemented on the robot and crane are presented. Then, a procedure for designing the robot's and crane's admittance parameters is given. The last part of the section shows a method to verify the stability of the whole system, i.e. robot admittance controller working together with the crane admittance controller.

3.1 Robot and crane admittance controllers

The admittance transfer functions on the robot and crane sides are integrated into a closed-loop and an open-loop system, respectively, see Figure 2. The selection of the robot admittance transfer function parameters must consider the closed-loop stability including the robot's dynamics. On the other hand, the crane admittance transfer function defines an open-loop system together with the crane dynamics, and the selection of the admittance parameters is mainly to shape the velocity command v_{ac} from the received force F. A closed-loop velocity control between the crane and its admittance seems a natural option but analyzing an open-loop system is better from a practical perspective as the closed hardware architecture of the cranes rarely provides velocity measurements.

The robot and crane admittance transfer functions of the scheme in Figure 2 can be represented as a second-order transfer function:

$$\frac{V_{a_i}(s)}{F(s)} = \frac{s}{M_i s^2 + B_i s + K_i} = \frac{s\omega_{n_i}^2/M_i}{s^2 + 2\zeta_i\omega_{n_i}s + \omega_{n_i}^2} \tag{3}$$

where s is the Laplace variable, ω_{n_i} is the natural frequency, and ζ_i is the damping coefficient. The subscript i refers to the coefficients of the robot admittance transfer function when $i = r$, and to the coefficients of the crane admittance transfer function when $i = c$. Then, the robot's admittance parameters are M_r, B_r and K_r, and the crane's admittance parameters are M_c, B_c and K_c.

From equation (3), the natural frequency ω_{n_i}, and the damping coefficient ζ_i can be written in terms of the admittance parameters M_i, B_i and K_i as follows, $\omega_{n_r} = \sqrt{\frac{K_r}{M_r}}$, $\zeta_r = \frac{B_r}{2\sqrt{M_r K_r}}$, $\omega_{n_c} = \sqrt{\frac{K_c}{M_c}}$, and $\zeta_c = \frac{B_c}{2\sqrt{M_c K_c}}$. Thus, the time response of the robot and crane admittance controllers is characterized by the values of ω_{n_r} and ζ_r, and ω_{n_c} and ζ_c, respectively. Therefore, the robot's admittance parameters M_r, B_r and K_r that provide a desired time response can be computed using equation (3). Also, the crane's admittance parameters M_c, B_c and K_c that give a desired time response can be computed using equation (3).

3.2 Robot's admittance control design

Consider the velocity-based admittance control in the block diagram in Figure 3 (Vukobratovic *et al.*, 2009). The robot's dynamics are studied using a velocity controller transfer function with time constant τ_r. The block K_e is the stiffness of the environment used to compute the force F in equation (2). From Figure 3, the transfer function from the input x_d to the output x_r is as follows:

$$\frac{X_r(s)}{X_d(s)} = \frac{s(M_r s^2 + B_r s + K_r)}{c_1 s^4 + c_2 s^3 + c_3 s^2 + c_4 s + c_5} \tag{4}$$

where $c_1 = \tau_r M_r$, $c_2 = \tau_r B_r + M_r$, $c_3 = \tau_r K_r + B_r$, $c_4 = \tau_r K_e + K$, $c_5 = K_e$ and s is the Laplace variable. The denominator in equation (4) is the characteristic equation of the system Dorf and Bishop (2022), and it provides information about the system's stability. When all the roots of $c_1 s^4 + c_2 s^3 + c_3 s^2 + c_4 s + c_5$ have the real part negative, one can conclude the system is stable.

The robot's admittance control parameters M_r, B_r and K_r are selected using the second-order system representation in equation (3), and the transfer function in equation (4) is used to verify stability.

Selecting a large value of damping coefficient ζ is a common approach to achieve a critical damping response avoiding oscillations during contact (Vukobratovic *et al.*, 2009). Then, a damping factor of $\zeta_r = 1$ is chosen to have a response with critical damping, and from the equation $\zeta_r = \frac{B_r}{2\sqrt{M_r K_r}}$, the mass M_r, the stiffness K_r and the damping B_r are linked by the equation:

$$B_r = 2\sqrt{M_r \cdot K_r}, \tag{5}$$

Using equation (5), the procedure to select the robot's admittance control parameters starts by choosing the value of the mass M_r, and a stiffness value K_r bigger than the environment stiffness K_e to have a rigid robot capable of moving the payload. Then, the damping B that gives a critical damping response is selected using equation (5).

The stability of the selected parameters should be tested using the characteristic equation in equation (4). A useful way to check stability is observing the location of the roots of the characteristic equation (4) when the parameters M_r, B_r and K_r change. For example, one can know how big the value of K_r has to be selected to preserve stability. The next numerical example shows how the root's location can be obtained, and how the system stability can be verified.

3.2.1 Numerical example

Considering the time constant $\tau_r = 0.02$, the environment's stiffness $K_e = 500$ (equivalent to a pendulum of mass $m = 100$ [kg], rope length $R = 2$ [m] and $g = 9.81$ [m/s^2], see Figure 7), and $M_r = 10$. Once the mass is fixed as $M_r = 10$, one can compute a set of damping values B_r from a set of K_r values using equation (5). The set of B_r and K_r values form a set of characteristic equations with roots located at different places of the imaginary and real axes. For example, for a set of values of $K_r = [1, 2, 3, \ldots, 100000]$, a set of values of B_r is obtained, and the roots location for the corresponding set of characteristic equations is presented in Figure 4. Three values of K_r are marked in in Figure 4. One value corresponds to $K_r = 1$ with roots located on the right side of the complex plane. The second value $K_r = 85.49$ is a critical value located on the imaginary axis, and the third value $K_r = 487.178$ corresponds to roots on the real axis. Therefore, one must avoid choosing $K_r < 85.49$ as the roots are located on the right side and instability is expected. On the other hand, choosing $K_r \geq 487.178$ produces a non-oscillatory response, and an oscillatory behavior is expected when $85.49 < K_r < 487.178$.

Figure 3 Block diagram of velocity-based admittance control

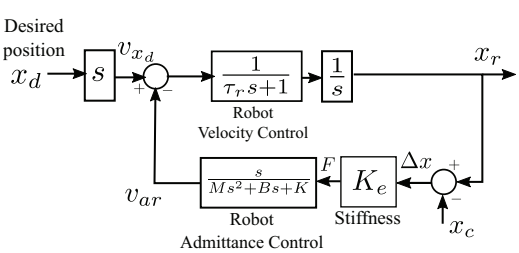

3.3 Crane's admittance control design

A similar approach can be followed to select the crane's admittance parameters M_c, B_c and K_c. In the crane's case, one should consider critical damping via $B_c = 2\sqrt{M_c \cdot K_c}$, and the crane dynamics using the transfer function:

$$\frac{X_c(s)}{V_{ac}(s)} = \frac{1}{s(\tau_c s + 1)}$$

where τ_c is the time constant corresponding to the crane's velocity control, $X_c(s)$ and $V_{ac}(s)$ are the crane's position x_c and velocity v_{ac} in the Laplace domain, respectively.

The transfer function from the force $F(s)$ to the crane's position $X_c(s)$ is as follows:

$$\frac{X_c(s)}{F(s)} = \frac{1}{(\tau_c s + 1)(M_c s^2 + B_c s + K_c)}, \tag{6}$$

obtained via the cascade connection of the crane's admittance transfer function in equation (3) and the transfer function of the crane dynamics $1/(s(\tau_c s + 1))$ (Figure 2).

Figure 4 Location of roots of the characteristic equation in equation (4) for different values of K_r and B_r with $M_r = 10$

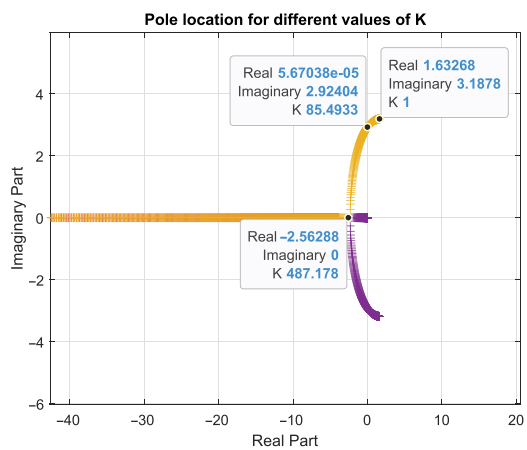

The mass M_c and stiffness K_c should be selected considering the robot's admittance parameters in the following way. The virtual mass M_c should be lighter than M_r to ensure the robot can push the payload. The stiffness K_c should be smaller than K_r to have a complaint crane that moves after the robot pushes the payload. The stability of the crane's admittance can be verified by analyzing the roots of the characteristic equation of transfer function in equation (6). The next example shows how to select the crane's admittance parameters and verify stability.

3.3.1 Numerical example

Consider the time constant $\tau_c = 0.1$, the environment's stiffness $K_e = 500$, and the robot's admittance parameters from the previous numeric example $M_r = 10$, $B_r = 283$, and $K_r = 2000$. Then, the selection of the crane's admittance parameters is the next. The mass $M_c = 1$ and the stiffness $K_c = 1000$ are selected smaller than M_r and K_r, respectively. The damping B_c is computed as $B_c = 2\sqrt{1 * 1000} = 64$. Using the selected parameters $M_c = 1$, $B_c = 64$ and $K_c = 1000$ in the characteristic equation of equation (6), the roots are $0, -32.5536, -30.6857, -10.0107$ and stability in the crane's admittance controller is expected.

3.4 Stability analysis of the collaborative scheme

The proposed scheme in Figure 2 can be analyzed using two mass-spring-damper models. One model is the equivalent mass-spring-damper system of the robot under admittance control, and the second model is the admittance of the crane. The two equivalent models are connected through the stiffness of the environment K_e (Figure 5).

The dynamics of the system presented in Figure 5 are defined by the next equations:

$$M_r\ddot{x}_r + B_r\dot{x}_r + K_r x_r = F_r + F \tag{7}$$

$$M_c\ddot{x}_c + B_c\dot{x}_c + K_c x_c = F \tag{8}$$

where x_r, M_r, B_r and K_r are the robot's position, the mass, the damping and the stiffness of the robot's admittance, respectively. The force produced by the robot's actuators is F_r, and F is the interaction force defined by the elastic model in equation (2) with environment stiffness K_e, and $\Delta = x_r - x_c$. The crane's position and its admittance parameters are x_c, M_c, B_c and K_c, respectively.

Considering initial conditions equal to zero, and applying the Laplace transform to equations (7) and (8), the transfer function from the force F_r to position x_c is the next one:

$$\frac{X_c(s)}{F_r(s)} = \frac{K_e}{s^4 + a_1 s^3 + a_2 s^2 + a_3 s + a_4} \tag{9}$$

Figure 5 Equivalent two-mass spring damper system

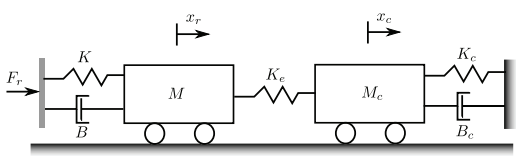

where s is the Laplace variable, and $X_c(s)$ and $F_r(s)$ are the crane's position x_c and the robot's force F_r in Laplace domain, respectively. The denomitator's coefficients are $a_1 = \frac{M_r B_c + B_r M_c}{M_r M_c}$, $a_2 = \frac{M_r K_c + M_r K_e + B_r B_c + K_r M_c - K_e M_c}{M_r M_c}$, $a_3 = \frac{B_r K_c + B_r K_e + K_r B_c - K_e B_c}{M_r M_c}$ and $a_4 = \frac{K_r K_c + K_r K_e - KeKc}{M_r M_c}$.

The transfer function in equation (9) is an input-output model of the collaborative scheme in Figure 2. Equation (9) describes how the crane's position x_c responds to the force F_r produced by the robot and transmitted to the payload via the interaction force F. The Routh–Hurtwitz stability criterion Dorf and Bishop (2022) can be used to verify the admittance parameters that ensure the stability of the whole scheme.

Considering the Routh–Hurtwitz stability criterion, and using the denominator coefficients of equation (9), the admittance parameters of the robot and the crane that ensure stability have to satisfy the next inequalities (Dorf and Bishop, 2022):

$$a_1 > 0; \quad a_3 > 0; \quad a_4 > 0 \quad a_1 a_2 a_3 > a_3^2 + a_1^2 a_4 \tag{10}$$

Finding an analytical solution for the inequalities in equation (10) is not straightforward; however, they can be implemented using a numeric computing software like Matlab, and the stability can be verified for selected admittance parameters. The next example shows how the inequalities in equation (10) are used to verify stability.

3.4.1 Numerical example

Considering the environment's stiffness $K_e = 500$, and the robot and crane admittance parameters from the previous examples $M_r = 10$, $B_r = 283$, $K_r = 2000$, $M_c = 1$, $B_c = 64$, $K_c = 1000$. The coefficients $a_1 = 92.3$, $a_2 = 3461.2$, $a_3 = 52050$ and $a_4 = 250000$ of the transfer function in equation (9) are computed. Then, the inequalities in equation (10) hold as $a_1 > 0$ $a_3 > 0$, $a_4 > 0$, and $a_1 a_2 a_3 > a_3^2 + a_1^2 a_4$ $(1.6 \times 10^{10} > 4.8 \times 10^9)$. Therefore, the stability of the whole collaborative scheme is concluded.

4. Numerical simulations and robot experiment

This section presents the validation of the proposed collaborative scheme via numeral simulations and experiments using a lightweight robot to push the payload and an industrial robot with a pendulum attached to its end effector to emulate the crane and payload.

4.1 Numerical simulations

To validate the functionality of the proposed collaborative scheme in Figure 2, the scheme is programmed in Simulink following the block diagram in Figure 6. The robot's dynamics is simulated as the velocity control transfer function with time constant τ_r, and an integrator to get the robot's position x_r. The crane's dynamics is simulated using the velocity control transfer function with time constant τ_r, and an integrator to get the crane's position x_c. Constant K_e is the environment's stiffness used to compute the interaction force F from $\Delta x = x_r - x_c$. The blocks robot and crane admittance transfer functions generate the velocities v_{ar} and v_{ac}, respectively. Note that the crane's position x_c is connected with the robot's loop to compute F for simulation purposes. In practice, the interaction force F is the only signal sent to the crane loop.

Figure 6 Simulation block diagram of the collaborative scheme

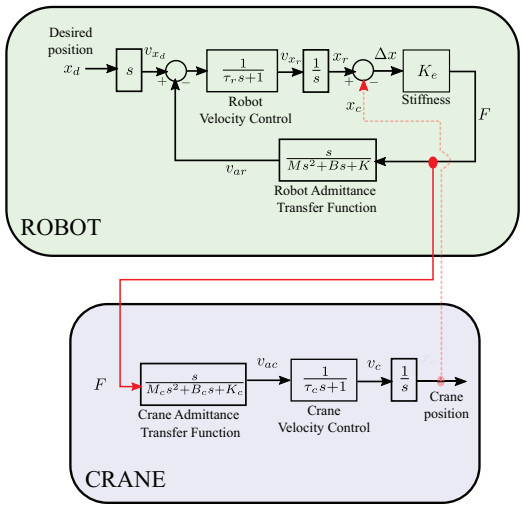

The simulation is performed using the following parameters. $\tau_r = 0.02$ and $\tau_c = 0.1$ are the time constants of the transfer functions representing the robot and crane velocity controllers, respectively. Considering a payload of mass $m = 100$ [kg] with a rope's length $R = 2$ [m], and the gravity $g = 9.81$ [m/s^2], the stiffness K_e equivalent to those parameters is estimated via equation (1). Using a set of values of L to get a set of values of F_h, a plot L vs F_h is obtained, and the value of $K_e = 500$ [N/m] is the slope of the plot's linear part (Figure 7).

The admittance parameters for the robot and crane are $M = 10$ [kg], $B = 2000$ [Ns/m], $K = 60000$ [N/m], $M_c = 1$ [kg], $B_c = 500$ [Ns/m] and $K_c = 1000$ [N/m]. One can verify that these admittance parameters satisfy the stability conditions (10).

The simulation lasts 20 s with a fixed sample time of 4 ms using Euler solver. The robot's velocity reference v_{x_d} is a trapezoidal velocity profile with a maximum velocity of approximately 0.1 [m/s].

Figure 7 Plot horizontal force F_h in equation (1) versus displacement L considering $m = 100$ [kg], $R = 2$ [m] and $g = 9.81$ [m/s^2]

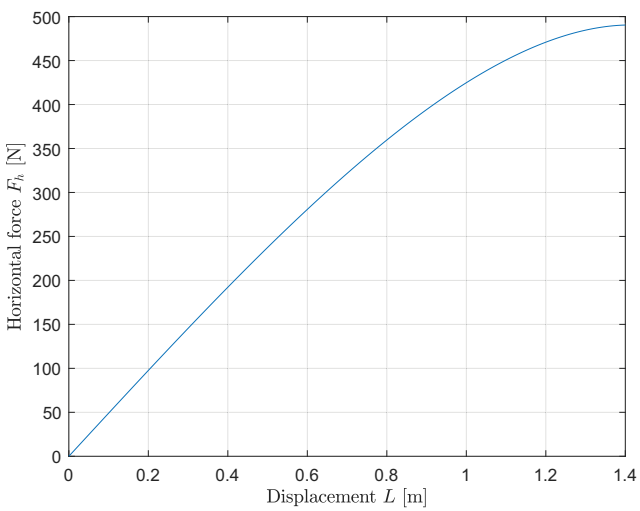

The robot velocity reference v_{x_d}, robot velocity v_{x_r}, contact force F, crane velocity command v_{ac}, and crane velocity v_c obtained from the numerical simulation are presented in Figure 8. The upper plot shows that the robot velocity v_{x_r} follows the velocity reference v_{x_d} exerting a force F of maximum 100 [N] on the payload. From the contact force F, the crane admittance transfer function produces a crane velocity command v_{ac} with a maximum velocity of 0.1 [m/s]. The crane velocity v_c follows the command v_{ac}.

From the numerical simulation results presented in Figure 8, one can conclude that the collaboration robot and crane is achieved since the crane moves according to the interaction force F generated by the robot pushing the payload.

Using Simscape, a 3D animation of the collaboration robot and crane is built inside the Simulink simulation. Figure 9 presents the animation including the robot end-effector, the rope, the payload, and the crane's trolley represented by the orange/black rectangular brick, the black straight line, the grey sphere, and the yellow square brick, respectively.

The frames in Figure 9 show the displacement of the robot's end-effector in contact with the payload, and the crane, when the trapezoidal profile presented in Figure 8 is applied to the robot. One can observe how the robot moves the payload

Figure 8 Simulation of the collaborative scheme with a maximum velocity 0.1 [m/s], $\tau_r = 0.02$ and $\tau_c = 0.1$

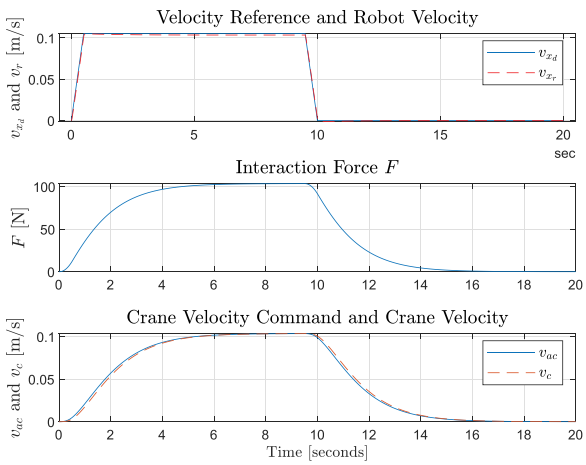

Note(s): Top: Robot velocity reference v_{x_d} and robot velocity v_{x_r}. Middle:contact force F. Bottom: crane velocity command vac andcrane velocity v_c

Figure 9 Frames of the 3D animation from Simscape

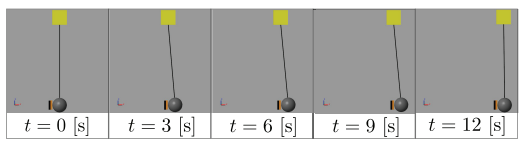

Note(s): The robot end-effector, the rope, the payload and the crane's trolley are represented by the orange/black rectangular brick, the black straight line, the gray sphere and the yellow square brick, respectively

producing a sway angle different than zero, and a position deviation with respect to the crane. Then the crane moves after the payload until they reach the final position. Therefore, the 3D animation confirms that the robot and the crane manipulate the payload collaboratively.

4.1.1 Collaborative scheme vs velocity control

A comparison of the collaborative scheme with only velocity commands in the crane and the robot is made to illustrate how pure velocity control might not be the best option for a collaboration robot-crane. Consider the previously used velocity time constant $\tau_r = 0.02$ for the robot, and a velocity time constant $\tau_c = 4$ slower than the previous one. The velocity control is tested by sending the same command v_{x_d} (used previously) to the robot and the crane omitting interaction forces and admittance control. Plots of the collaborative scheme and the velocity control simulation are presented in Figure 10 (a–c), and Figure 10 (d–f), respectively. The interaction force F and the crane's velocity v_c are the main differences between the two approaches, see Figure 10 (b and c) and 10 (e and, f).

From Figure 10(b) and Figure 10(e), one can observe that the velocity control generates an interaction force F bigger than the proposed collaborative scheme. Comparing crane velocity v_c in Figure 10(c) and Figure 10(f), the presented collaborative scheme makes the crane move faster and follows the interaction force despite the slow dynamics of the crane. One can observe that the crane admittance control shapes the velocity command v_{ac} to generate a crane velocity v_c that follows the interaction force.

4.2 Robot experiment

The proposed collaborative scheme is tested using the experimental setup in Figure 11. The crane and payload are emulated by attaching a pendulum on an industrial robot KUKA KR 210 R2700 (Quantec). The attached mass and the length of the rope are $m = 10$ [kg] and $R = 0.5$ [m], respectively. The robot used to move the payload is a KUKA LBR iiwa 14 R820.

Figure 12 shows a block diagram of collaborative scheme implementation. The crane is controlled with Cartesian velocity commands sent through a PLC interface. SW-in-the-Loop (SIL) approach was applied, and a Matlab/Simulink interface Safeea and Neto (2023) is used to send the robot's end-effector Cartesian position increments and receive the measured contact force F using UDP protocol. The robot and crane admittance are implemented inside the Matlab/Simulink to send corrections to the robot and velocity commands v_{ac} to the crane, respectively. The sampling time used in all the experiments is set to 4 ms.

From the mass $m = 10$ [kg] and length $R = 0.5$ [m] of the pendulum attached to the industrial robot, the estimated stiffness is $K_e = 200$ [N/m]. The admittance parameters for the robot and crane used in the experimental test are $M = 10$ [kg], $B = 1000$ [Ns/m], $K = 2000$ [N/m], $M_c = 1$ [kg], $B_c = 500$ [Ns/m] and $K_c = 600$ [N/m]. Three trapezoidal velocity profiles commanded to the robot are tested and the experimental results are presented in Figure 13. The maximum velocities of the velocity commands are 0.15, 0.09 and 0.045 m/s. The robot velocity reference v_{x_d}, the robot velocity v_{x_r}, the contact force F, the crane velocity command v_{ac} and the velocity crane v_c data was recorded and plotted in Figure 13. Plots A1-A3, B1-B3 and C1-C3 correspond to the velocity commands 0.15, 0.09 and 0.045 m/s, respectively. From Figure 13, one can see that the robot and crane move together

Figure 10 Simulation of the collaborative scheme and velocity control with a maximum velocity 0.1 [m/s], $\tau_r = 0.02$ and $\tau_c = 4$

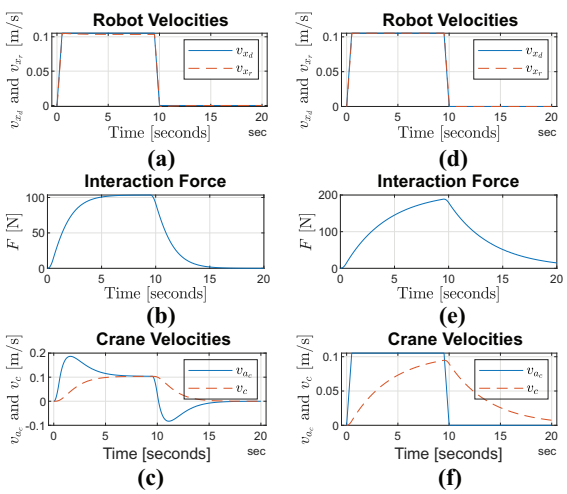

Figure 11 Experimental setup: KUKA KR 210 R2700 with attached pendulum emulates the crane, and KUKA LBR iiwa 14 R820 is the robot

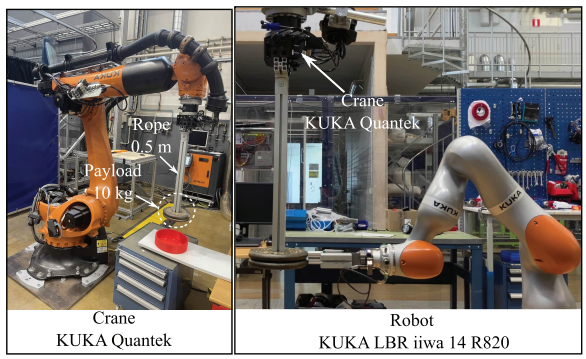

Figure 12 Implementation of the proposed scheme on the experimental setup

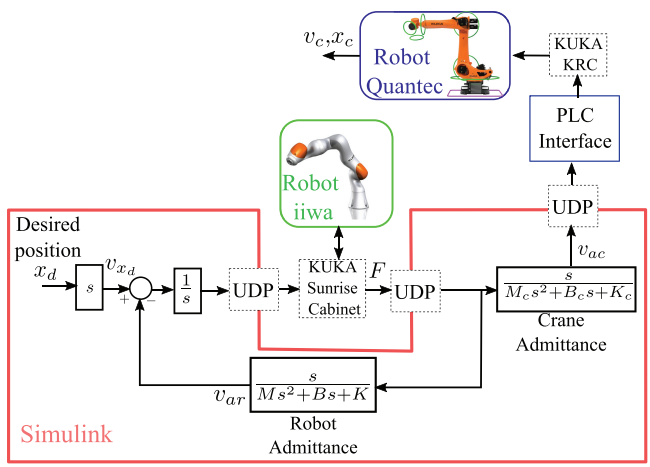

Figure 13 Robot velocity reference v_{x_d}, Force F, and crane velocity command v_{ac} and crane velocity v_c from experimental results

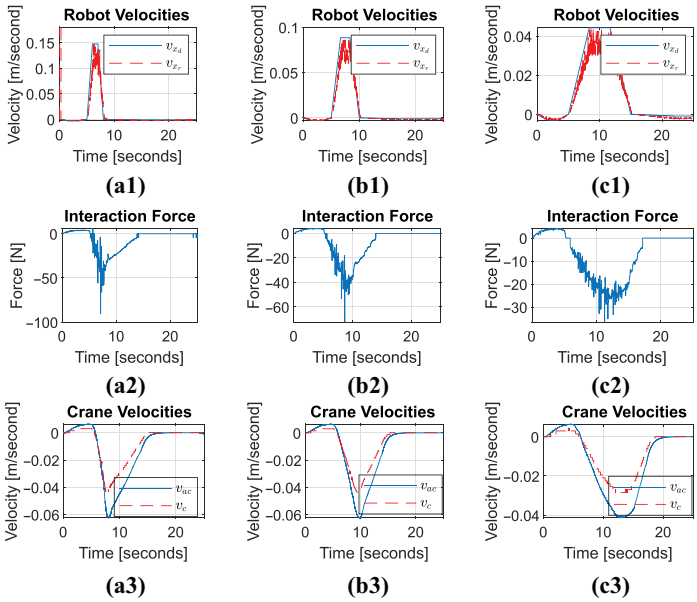

Note(s): Plots a1-a3, b1-b3 and c1-c3 correspond to the velocity commands 0.15, 0.09 and 0.045 m/s, respectively

following the velocity profile and the velocity command generated by the interaction force F, respectively.

Figure 14 shows six video frames taken during the test corresponding to the 0.045 m/s profile. One can see the robot and crane moving collaboratively with the payload.

A two-dimensional test in x and z directions is presented in Figure 15. Four independent admittance controllers are implemented, i.e. two for the robot to cover x_r and z_r directions, and two for the crane to cover x_c and z_c directions. Figure 15 (a and b), presents the interaction force and crane velocity command v_{ac} in the x-direction, when a velocity profile of 0.09 [m/s] is sent to the robot. Figure 15 (c and d), shows the robot's vertical pulling interaction force and crane velocity commands in the z direction. Typically, movement along the z-axis is slow to ensure precise assembly operations. With the crane admittance parameters set to $M_{\text{crane}} = 1$ kg, $K_{\text{crane}} = 200$ N/m, and $B_{\text{crane}} = 500$ Ns/m, the interaction force was approximately 5 N, while the maximum velocity reached 0.015 m/s.

Figure 14 Experiment's frames of the robot-crane collaboration

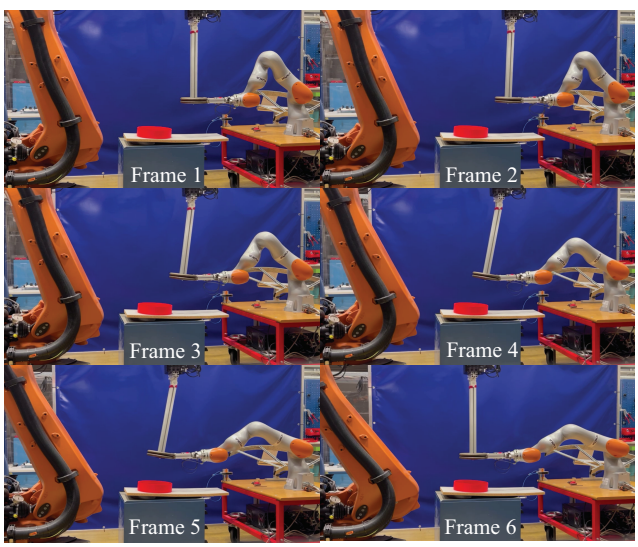

Figure 15 Experimental results of two-dimensional test

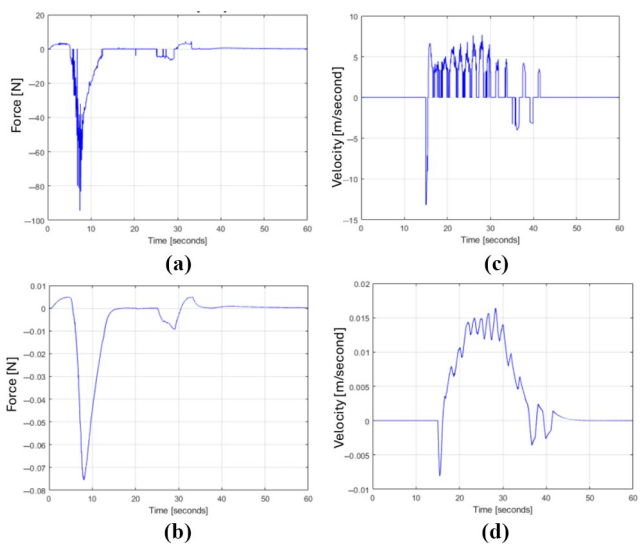

Note(s): Force F and crane velocity command v_{ac} of x-direction and z-direction are presented in the plots (a) and (b), and (c) and (d), respectively

5. Discussion

From Figures 10 and 13, one can observe the force-based manipulation of the payload, i.e. whenever the lightweight robot exerts a force on the payload, the other robot (emulating the crane) moves with a velocity directly proportional to the exerted force. The results presented in this paper are a proof of concept of the future implementation on the real crane. Some actions need to be considered before the final implementation. First, the experiments presented in this manuscript are limited to a two-dimensional case, and an extension to a three-dimensional case is needed to have a closer approach to the real work. Second, the velocity controllers of the real-world cranes have nonlinearities, such as dead zones. Then, the velocity command of the crane is perceived as zero velocity when its value is under a certain limit; this must be considered during the design of the crane's admittance controller. Furthermore, it is worth mentioning that the motion in the vertical direction is more challenging since the effect of the payload's weight on the interaction force is stronger in this direction, and this perturbs the velocity commands to the crane; this must be considered during the design of the crane's admittance controller, too.

The presented collaborative scheme aims to relocate the operator to a risk-free area, far enough from the payload to ensure her/his safety, and to integrate the scheme directly into already-operational cranes that may not have an angle sensor. Therefore, we execute all the tests without integrating an IAD and a sway angle measurement in our experimental setup. A pending action before a full integration of the proposed collaborative scheme into the real-world crane is to perform a comparison with other handle/lever-based IAD and manual operation to analyze metrics such as sway angle suppression, task completion, positioning accuracy and/or operator effort.

6. Conclusions

An effective robot-crane collaborative control scheme for manipulating heavy payloads is presented. The scheme is a safe approach since the operator is not in contact with the heavy object, and compliance is considered in the robot and the crane to limit the interaction forces. The simulations and experiments using an industrial robot to emulate the crane and a lightweight robot to manipulate the payload verified the functionality of the approach.

Future work will be the extension from two-dimensional *xz* motion to three dimensions *xyz*, and a test on the real crane. Also, eye-to-hand visual servoing will be integrated to get the payload's desired location and to control the robot using visual feedback.

References

Ambrosino, M., Boucher, F., Mengeot, P. and Garone, E. (2022), "Constrained control scheme for the manipulation of heavy pre-fabricated elements with lightweight robotic arm", in T. Linner, B. GarcÃa de Soto, R. Hu, I. Brilakis, T. Bock, W. Pan, A. Carbonari, D. Castro, H. Mesa, C. Feng, M. Fischer, C. Brosque, V. Gonzalez, D. Hall, M. S. Ng, V. Kamat, C.-J. Liang, Z. Lafhaj, W. Pan, M. Pan and Z. Zhu (Eds), *Proceedings of the 39th International Symposium on Automation and Robotics in Construction, International Association for Automation and Robotics in Construction (IAARC), Bogotá, Colombia*, pp. 383-390.

Ambrosino, M., Boucher, F., Mengeot, P. and Garone, E. (2024), "Experimental validation of a constrained control architecture for a multi-robot bricklayer system", *Mechatronics*, Vol. 98, p. 103139.

Arai, T., Osumi, H. and Ohta, J. (1988), "Crane control system with an industrial robot", *in* R. Ishikawa, ed., '*Proceedings of the 5th International Symposium on Automation and Robotics in Construction (ISARC)', International Association for Automation and Robotics in Construction (IAARC), Tokyo, Japan*, pp. 747-754.

Bey-Temsamani, A., Schouterden, G., Van den Bergh, J., Meskens, J., Incirci, T. and Kellens, K. (2022), "Intelligent overhead crane improves operator ergonomics and productivity", *Procedia CIRP*, Vol. 106, pp. 132-137.

Bicchi, A., Peshkin, M.A. and Colgate, J.E. (2008), "Safety for physical human-robot interaction", *Springer Handbook of Robotics*, Springer, Berlin, Heidelberg, pp. 1335-1348.

Campeau-Lecours, A., Foucault, S., Laliberté, T., Mayer-St-Onge, B. and Gosselin, C. (2016), "A cable-suspended intelligent crane assist device for the intuitive manipulation of large payloads", *IEEE/ASME Transactions on Mechatronics*, Vol. 21 No. 4, pp. 2073-2084.

Campeau-Lecours, A., Belzile, P.-L., Laliberté, T., Foucault, S., Mayer-St-Onge, B., Gao, D. and Gosselin, C. (2017), "An articulated assistive robot for intuitive hands-on-payload manipulation", *Robotics and Computer-Integrated Manufacturing*, Vol. 48, pp. 182-187.

Dorf, C.R. and Bishop, R.H. (2022), "Modern control systems", Pearson Education Limited, Harlow.

Heuer, C. and Brell-Cokcan, S. (2025a), "Adaptive robotic platform for the installation of refurbishment panels", *Construction Robotics*, Vol. 9 No. 2, p. 17.

Heuer, C. and Brell-Cokcan, S. (2025b), "Automated multi-agent assembly: collaborative robot-crane concept and capability matching implementation for the automated assembly of heavy construction components", *in* Huber, M., Verl, A. and Kraus, W. (Eds), *'European Robotics Forum 2025'*, Springer Nature Switzerland, Cham, pp. 95-100.

Hoffman, R. and Asada, H.H. (2020), "Precision assembly of heavy objects suspended with multiple cables from a crane", *IEEE Robotics and Automation Letters*, Vol. 5 No. 4, pp. 6876-6883.

Hoffman, R. and Asada, H.H. (2021), "Control strategy for jam and wedge-free 3D precision insertion of heavy objects suspended with a multi-cable crane", *IEEE Robotics and Automation Letters*, Vol. 6 No. 4, pp. 7453-7460.

Kazuo, F. and Shinsaku, T. (1995), "Lifted cargo positioning device", available at: https://patents.google.com/patent/JPH0710464A. JPH0710464A

Kazuo, F., Yasuo, T. and Shinsaku, T. (1994), "Positioning robot, device for positioning suspended load and device for detecting relative position", available at: https://patents.google.com/patent/JPH06312386A. JPH06312386A

Krüger, J., Lien, T.K. and Verl, A. (2009), "Cooperation of human and machines in assembly lines", *CIRP Annals*, Vol. 58 No. 2, pp. 628-646.

Liu, C., Wu, J., Jiang, X., Gu, Y., Xie, L. and Huang, Z. (2024), "Automatic assembly of prefabricated components based on vision-guided robot", *Automation in Construction*, Vol. 162, p. 105385.

O'Neill, C. and Asada, H.H. (2021), "Safe tumbling of heavy objects using a two-cable crane", *IEEE Robotics and Automation Letters*, Vol. 6 No. 2, pp. 1082-1089.

O'Neill, C. and Asada, H.H. (2022), "Horizontal insertion of a ring onto a shaft using a gantry crane with minimal sensors", *IEEE Robotics and Automation Letters*, Vol. 7 No. 3, pp. 7271-7278.

Peng, K.C.C., Singhose, W., Gessesse, S. and Frakes, D. (2009), "Crane operation using hand-motion and radio frequency identification tags", in *'2009 IEEE International Conference on Control and Automation'*, pp. 1110-1115.

Safeea, M. and Neto, P. (2023), "Model-based hardware in the loop control of collaborative robots: simulink and python based interfaces", *International Journal of Computer Integrated Manufacturing*, Vol. 0 No. 0, pp. 1-13.

Schubert, P., Stemmler, S. and Abel, D. (2019), "Development of a human machine interface for crane-based load handling using a lightweight robot", *'2019 27th Mediterranean Conference on Control and Automation (MED)'*, pp. 292-298.

Siciliano, B., Sciavicco, L., Villani, L. and Oriolo, G. (2009), *Robotics: Modelling, Planning and Control*, Springer, London.

Vukobratovic, M., Surdilovic, D., Ekalo, Y. and Katic, D. (2009), *Dynamics and Robust Control of Robot-Environment Interaction*, World Scientific Publishing, Singapore, Vol. 2.

Welch, H., Mohan, S., Santillo, M. and Mazumdar, A. (2022), "Intelligent push-pull devices for manipulation of slung loads", *IEEE Robotics and Automation Letters*, Vol. 7 No. 2, pp. 5294-5301.

Yutaka, U. and Motohisa, H. (1994), "Positioning device for large weight article by cooperation of crane and robot", available at: https://patents.google.com/patent/JPH06218685A. JPH06218685A

Further reading

Haninger, K., Radke, M., Vick, A. and Krüger, J. (2022), "Towards high-payload admittance control for manual guidance with environmental contact", *IEEE Robotics and Automation Letters*, Vol. 7 No. 2, pp. 4275-4282.

Corresponding author

Antonio Rosales can be contacted at: antonio.rosales@vtt.fi